ACI STRUCTURAL JOURNAL TECHNICAL PAPER

Title No. 113-S91

Earthquake-Resistant Squat Walls Reinforced with High-Strength Steel

by Min-Yuan Cheng, Shih-Ching Hung, Rémy D. Lequesne, and Andrés Lepage

Results are reported from reversed cyclic tests of five large-scale squat wall specimens reinforced with steel bars having a specified yield strength of either 60 or 115 ksi (413 or 792 MPa). Two specimens were designed for a shear stress of $5\sqrt{f_c'}$ psi ($0.42\sqrt{f_c'}$ MPa) and the other three $9\sqrt{f_c'}$ psi ($0.75\sqrt{f_c'}$ MPa). Boundary element confining reinforcement complied with the requirements of Chapter 18 of ACI 318-14 in all but one specimen, which had 50% of the required transverse boundary element reinforcement. Specimens constructed with Grade 115 steel had similar strength and exhibited 20% greater drift capacity than those with Grade 60 steel. Use of Grade 115 steel tended to control the softening effect of sliding at the base of the wall and to increase the component of drift due to reinforcement strain penetration into the foundation.

Keywords: crack width; deformation capacity; displacement reversals; low-rise wall; shear strength.

INTRODUCTION

Reinforced concrete (RC) shear walls have substantial lateral stiffness and strength, and are thus commonly used as part of the lateral bracing system for buildings located in regions of high seismicity. For low- to mid-rise buildings, RC shear walls are often more cost-effective than RC moment-resisting frames (Moehle et al. 2011). Squat shear walls, with aspect ratios h_w/ℓ_w less than approximately 2, are common in low-rise structures, nuclear power plants, and tall buildings where the lateral bracing system is disrupted near the base to accommodate large open spaces.

The behavior of squat shear walls under reversed cyclic loads is heavily influenced by shear (Barda et al. 1977; Paulay et al. 1982). Per Chapter 18 of ACI 318-14 (ACI Committee 318 [2014]), Eq. (1) can be used to calculate the nominal web shear strength of walls, where $\alpha_c = 3$ (0.25 for metric) for walls with $h_w/\ell_w \le 1.5$. Chapter 18 also requires that web reinforcement ratios, ρ_t and ρ_ℓ, both exceed 0.0025.

$$V_{n1} = A_{cv}\left(\alpha_c\sqrt{f_c'} + \rho_t f_y\right) \le 10\sqrt{f_c'}A_{cv}, \text{ psi} \quad (1a)$$

$$V_{n1} = A_{cv}(\alpha_c\sqrt{f_c'} + \rho_t f_y) \le 0.83\sqrt{f_c'}A_{cv}, \text{ MPa} \quad (1b)$$

After reversing loads induce repeated yielding of wall reinforcement, concentrated deformations typically develop near the wall base (Paulay et al. 1982) that are associated with decay in strength and limited the lateral wall deformation capacity. For simplicity, the lateral strength of squat walls has thus been characterized using a shear-friction analogy (Wood 1990), wherein vertical reinforcement perpendicular to the base of the wall is assumed to provide the lateral resistance. ACI 318-14 defines the minimum nominal resistance to shearing along a cold joint, such as that at the base of a squat wall, with Eq. (2).

$$V_{n2} = 0.6A_{vf}f_y \le \min(0.2f_c'A_{cv}, (480 + 0.08f_c')A_{cv}, 1600A_{cv}), \text{ psi} \quad (2a)$$

$$V_{n2} = 0.6A_{vf}f_y \le \min(0.2f_c'A_{cv}, (3.3 + 0.08f_c')A_{cv}, 11A_{cv}), \text{ MPa} \quad (2b)$$

Equation (2), however, was not developed for members under reversing lateral loads and does not necessarily represent the concentrated deformations associated with concrete deteriorating after multiple cycles. Equation (3) (Wood 1990), which has a form similar to Eq. (2), has been shown to provide a lower-bound estimate of squat wall lateral force resistance (Gulec et al. 2008).

$$6\sqrt{f_c'}A_{cv} \le V_{n3} = 0.25A_{vf}f_y \le 10\sqrt{f_c'}A_{cv}, \text{ psi} \quad (3a)$$

$$0.5\sqrt{f_c'}A_{cv} \le V_{n3} = 0.25A_{vf}f_y \le 0.83\sqrt{f_c'}A_{cv}, \text{ MPa} \quad (3b)$$

Gulec et al. (2008) conducted a review of existing methods for calculating the lateral shear strength of squat walls using an extensive database of test results. Their findings indicated that current equations do not accurately estimate the shear strength of rectangular and flanged squat walls. An empirical relation (Eq. (4)) was proposed as an improved method for calculating the mean shear resistance of rectangular squat walls with aspect ratios of 1.0 or less (Gulec and Whittaker 2011).

$$V_{n4} = \frac{1.5\sqrt{f_c'}A_{cv} + 0.25F_{vw} + 0.2F_{vbe} + 0.4P}{\sqrt{h_w/\ell_w}} \le 10\sqrt{f_c'}A_{cv}, \text{ psi} \quad (4a)$$

$$V_{n4} = \frac{0.125\sqrt{f_c'}A_{cv} + 0.25F_{vw} + 0.2F_{vbe} + 0.4P}{\sqrt{h_w/\ell_w}} \le 0.83\sqrt{f_c'}A_{cv}, \text{ MPa} \quad (4b)$$

Equations (3) and (4) were developed using databases where the reported yield stress of the wall vertical reinforce-

ACI Structural Journal, V. 113, No. 5, September-October 2016.
MS No. S-2015-322.R1, doi: 10.14359/51688825, received September 17, 2015, and reviewed under Institute publication policies.

ment did not exceed 90 ksi (620 MPa). There is increasing interest in the use of high-strength steel (HSS) reinforcement having f_y as high as 120 ksi (827 MPa) in structures located in earthquake-prone regions (NIST GCR 14-917-30 [2014]). Results from reversed cyclic load tests of squat walls reinforced entirely with steel having f_y = 95 ksi (655 MPa) and designed to fail in web shear (Eq. (1)) were recently published (Park et al. 2015). Specimens reinforced with conventional Grade 60 and HSS exhibited similar deformation capacity (approximately $0.01h_w$). Although it was shown that current design equations (Chapter 18 of ACI 318-14) for the shear strength of walls underpredicted the measured strength by a large margin, the specimens were not typical of U.S. practice, with wall boundary element reinforcement ratios of 9.7% and imposed shear stresses up to $20\sqrt{f_c'}$ psi ($1.67\sqrt{f_c'}$ MPa).

In addition to the use of HSS, there is interest in whether squat walls require the same boundary element confinement reinforcement as slender walls. Given that flexural deformations are less dominant in squat walls than in slender walls, well-confined boundary elements may be less essential to squat wall performance as long as the spacing of the transverse reinforcement in the boundary elements is sufficient to prevent premature buckling of the vertical bars.

Several issues thus remain unresolved, including whether: 1) the deformation capacity of squat walls is impacted by use of HSS; 2) current shear design provisions are appropriate for designing squat walls reinforced with HSS; 3) the minimum web reinforcement ratio can be reduced as f_y is increased; and 4) it is feasible to reduce the amount of transverse boundary element confinement reinforcement. To address these issues, five squat walls with h_w/ℓ_w = 1.0 and constructed with varied reinforcement yield strengths and target shear stresses were tested under reversed cyclic loads.

RESEARCH SIGNIFICANCE

This paper reports results from the first tests of squat walls reinforced primarily with HSS having f_y in excess of 100 ksi (689 MPa). The effect of using such high-strength reinforcement on the deformation capacity and shear resistance of walls is investigated. Use of HSS with a web reinforcement ratio below the ACI Building Code minimum is evaluated. In addition, results from the test of a specimen with reduced boundary element confining steel are compared with results from tests of walls compliant with ACI 318-14.

EXPERIMENTAL PROGRAM

Test specimens

Five specimens with aspect ratios h_w/ℓ_w of 1.0 were tested (Fig. 1). The specimens were constructed with nominal 6 ksi (41 MPa) concrete and reinforced with either Grade 60 or 115, f_y = 60 or 115 ksi (413 or 785 MPa). The Grade 115 steel used in this study complied with Japanese specifications for USD785 reinforcement (Aoyama 2001). Each specimen was constructed using a single grade of steel for horizontal and vertical reinforcement, except that Grade 60 steel was used as boundary element hoops in all specimens. Specimens designed for the same target strength had reinforcement ratios based on the value of f_y (that is, ρf_y was approximately constant).

Specimens labeled with letters "M" and "H" were designed for target shear stresses of 5 and $9\sqrt{f_c'}$ psi (0.42 and $0.75\sqrt{f_c'}$ MPa), respectively. Specimens H60, H115, and H60X were therefore designed for high ("H") shear stresses approaching the upper limit permitted by the ACI 318-14 of $10\sqrt{f_c'}$ psi ($0.83\sqrt{f_c'}$ MPa). The target shear strength of the specimens was based on V_{Mpr}, the shear associated with the probable moment, M_{pr}, which was determined assuming a rectangular compression zone stress block and a reinforcement stress of $1.25f_y$. Specimens were therefore designed aiming for their lateral strength to be limited by flexure. In Table 1, the target shear stress of all test specimens is presented.

Specimens were designed to have calculated shear strengths approximately equal to but greater than V_{Mpr} (Table 1). For design, the web shear strength of the specimens (V_{n1}) was calculated according to Eq. (1), with α_c = 3. All specimens had two curtains of web reinforcement with a spacing that varied depending on the shear demand and f_y. Web reinforcement consisted of No. 3 (10 mm) bars in Specimens M60 and M115 and No. 4 (13 mm) bars in the others.

For Specimen M60, reinforced with Grade 60 reinforcement, the horizontal web reinforcement required to resist shearing forces resulted in $\rho_t = \rho_\ell = 0.0031$ based on Eq. (1). This exceeded the minimum of 0.0025 required by ACI 318-14 for walls classified as "Special Structural Walls." Specimen M115, which was designed for approximately the same shear demand but reinforced with Grade 115 steel, $\rho_t = \rho_\ell = 0.0015$ was provided. This was less than the ACI 318-14 minimum, but provided approximately the same $\rho_t f_y$ as in Specimen M60.

Specimens M60, M115, H60, and H115 had No. 3 Grade 60 hoops spaced at 2.5 in. (65 mm) for confinement of the boundary elements. This spacing, equal to one-third of the wall thickness, satisfied all ACI 318-14 requirements for walls classified as "Special Structural Walls." In these specimens, the spacing of hoops also satisfied the maximum spacing of $4d_b$ recommended in NIST GCR 14-917-30 (2014) when using longitudinal bars of Grade 100 (690 MPa) or stronger. For Specimen H60X, the spacing of boundary element hoops was increased to 5 in. (130 mm), nearly two-thirds of the wall thickness. This spacing was approximately equal to $6d_b$, and was selected to delay buckling of longitudinal reinforcement.

Experimental setup and instrumentation

The specimens were tested under single curvature using the experimental setup shown in Fig. 2. The concrete base block was fixed to the strong floor using eight 2.7 in. (69 mm) diameter HSS threaded rods. Each rod was prestressed to approximately 360 kip (1600 kN) prior to testing. Lateral displacements were applied to the top of the wall through two steel-transfer beams clamped to either side of the top concrete block. The steel-transfer beams were connected to three 220 kip (980 kN) hydraulic actuators through a steel spreader beam (Fig. 2). The steel transfer beams were also

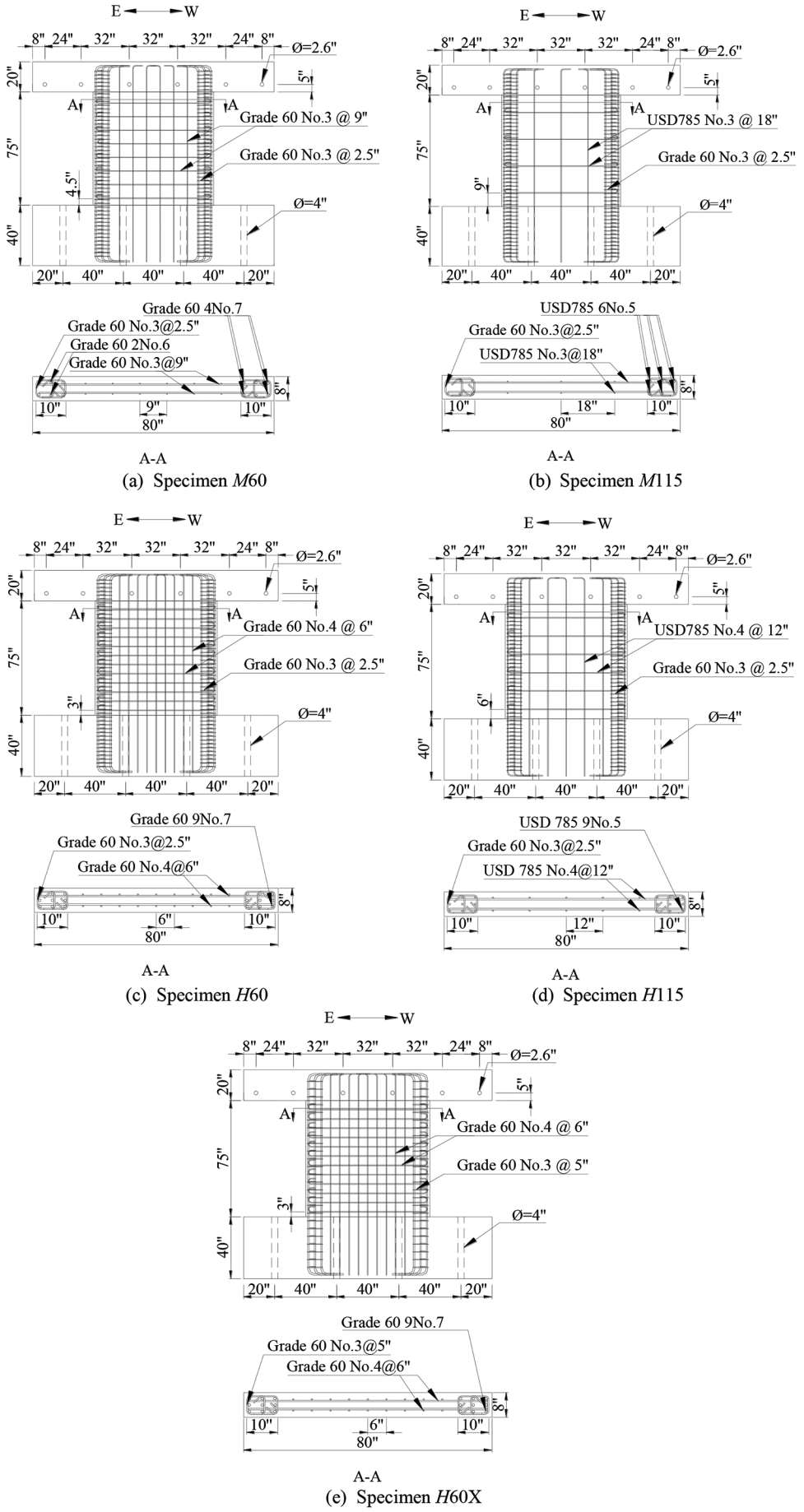

Fig. 1—Nominal dimensions and reinforcement layout for test specimens. (Note: 1 in. = 25.4 mm.)

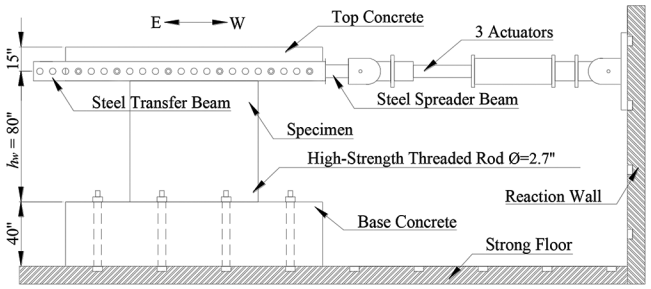

Fig. 2—Experimental setup. (Note: 1 in. = 25.4 mm.)

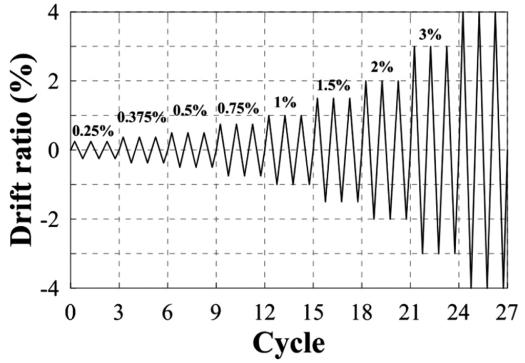

Fig. 3—Loading history.

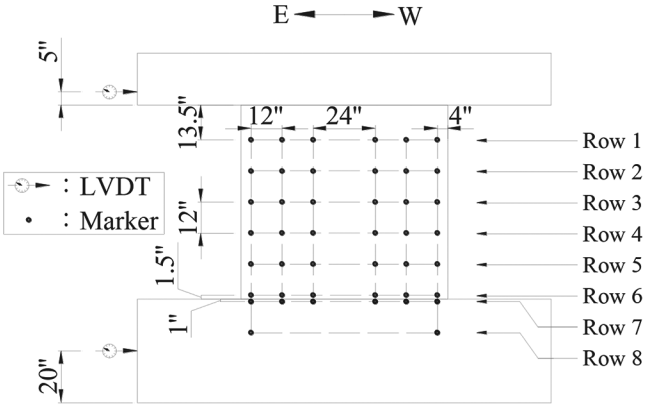

Fig. 4—Location of instrumentation for measurement of displacements. (Note: 1 in. = 25.4 mm.)

braced by lateral supports to prevent out-of-plane movement during the test.

The displacement-controlled actuators imposed the loading history shown in Fig. 3. The target drift ratio was defined as the lateral displacement of the actuator divided by h_w. A positive drift ratio corresponds to the actuator moving eastward.

Deformation of the specimens was recorded with linear variable differential transformers (LVDTs) and an infra-red-based noncontact system that tracked the position of multiple points referred to as "markers." The location of LVDTs and markers is shown in Fig. 4. Two LVDTs were used to measure the lateral movement of the concrete blocks: one was installed at the height of load application and the other at mid-height of the concrete base block. Forty-four markers were also used, with 36 of them attached to the specimen on a 12 in. (30 mm) grid pattern and the others

Table 1—Design parameters for test specimens

Specimen*†	M60	M115	H60	H115	H60X
f_y, ksi (MPa)	60 (413)	115 (785)	60 (413)	115 (785)	60 (413)
$\frac{V_{n1}}{A_{cv}\sqrt{f'_c}}$, psi	5.37 (0.45)	5.26 (0.44)	9.46 (0.79)	9.20 (0.77)	9.46 (0.79)
$\frac{V_{n2}}{A_{cv}\sqrt{f'_c}}$, psi	5.74 (0.48)	6.05 (0.50)	10.4 (0.87)	10.4 (0.87)	10.4 (0.87)
$\frac{V_{Mpr}}{A_{cv}\sqrt{f'_c}}$, psi	5.35 (0.45)	5.45 (0.45)	9.37 (0.78)	9.11 (0.76)	9.37 (0.78)
Spacing of hoops	$3.3d_b$	$4.0d_b$	$2.9d_b$	$4.0d_b$	$5.7d_b$

*All values are nominal.

†Nominal f_c' is 6 ksi (41 MPa) for all specimens.

fixed to the concrete base block. Steel strains were measured using 35 strain gauges per specimen.

Materials

The specimens were all cast on the same day using concrete from two concrete trucks. Specimens M60 and M115 were cast from the first truck and Specimens H60, H115, and H60X were cast from the other. The concrete mixtures had a specified compressive strength of 6 ksi (41 MPa) and a maximum aggregate size of 1 in. (25 mm). The reported concrete compressive strength (Table 2) is the average strength of three 4 x 8 in. (100 x 200 mm) concrete cylinders tested on the same day as the wall specimens.

Sample stress-strain curves, obtained for each type and size of steel through direct tensile tests, are shown in Fig. 5. The mechanical properties of the steel reinforcement are summarized in Table 2. The onset of the yield plateau was used to determine f_y because both the Grade 60 and 115 steel exhibited distinct yield plateaus (Fig. 5). The reported steel strain was measured using a gauge length of 8 in. (200 mm). Each value in Table 2 represents an average of values measured from tests of three samples, except that only two samples were available for the Grade 60 No. 6 bars and only one was available for Grade 60 No. 7 bars.

EXPERIMENTAL RESULTS

Overall response

The response of each specimen is plotted in Fig. 6 as $v_{test}/\sqrt{f'_c}$ versus drift ratio and results are summarized in Table 3. The drift ratio was calculated as the relative displacement between the top and bottom blocks, divided by h_w, and adjusted for rotation of the concrete base block calculated using data from the topmost row of markers on the base block (Fig. 4). Because the loading protocol was controlled by the actuator displacement, the actual drift ratios attained during the tests deviated from the intended loading history (Fig. 3). Unless specified as target drift, the drift used hereafter refers to the actual drift.

The responses of specimens reinforced with Grade 60 and Grade 115 (413 and 785 MPa) steel were similar. There were minor differences in the strength of the specimens and

Table 2—Material properties

Concrete cylinder strength					
Specimen	M60	M115	H60	H115	H60X
f_c', ksi (MPa)	5.7 (39)	5.5 (38)	6.4 (44)	6.4 (44)	6.1 (42)

Steel tensile properties							
Grade	Grade 115 (785)			Grade 60 (420)			
Bar size	No. 3 (10 mm)	No. 4 (13 mm)	No. 5 (16 mm)	No. 3 (10 mm)	No. 4 (13 mm)	No. 6 (19 mm)	No. 7 (22 mm)
f_y, ksi (MPa)	114 (786)	117 (806)	112 (770)	66 (453)	69 (475)	64 (440)	65 (450)
f_t, ksi (MPa)	136 (940)	147 (1010)	142 (980)	99 (684)	97 (666)	94 (647)	95 (653)
ε_{su}	0.083	0.085	0.080	0.12	0.12	0.13	0.14
ε_{sf}	0.10	0.10	0.10	0.15	0.16	0.19	0.17
f_t/f_y	1.20	1.25	1.27	1.51	1.40	1.47	1.45

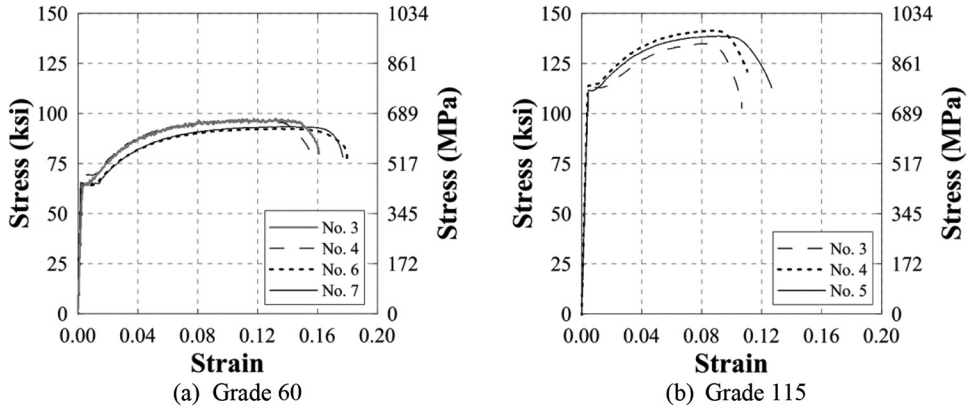

Fig. 5—Sample steel tensile stress-strain curves.

overall character of the measured hysteresis. Specimens reinforced with Grade 115 reinforcement tended to lose strength somewhat more gradually and exhibited approximately 20% greater deformation capacity d_u than those reinforced with Grade 60 reinforcement. As expected, shear stress had a strong influence on behavior, with Specimens H60 and H115 exhibiting an approximately 40% reduction in drift capacity compared to Specimens M60 and M115, regardless of reinforcement grade. This is clear in Fig. 6, where a circle identifies the peak of the first cycle to 3% drift ratio, showing that Specimens H60, H115, and H60X experienced a severe strength reduction before 3% drift, unlike Specimens M60 and M115. The hysteresis for Specimens H60 and H60X are nearly identical, indicating that doubling the spacing (and thus halving the area) of boundary element confinement reinforcement was not detrimental to lateral strength or deformation capacity.

Progression of damage

Cracking of the specimens progressed in a similar manner. Inclined (shear) and horizontal (flexural) cracks developed in all specimens during the first cycle to a target drift ratio of 0.25%. Cracks continued to form as the target drift ratio was increased up to 1%. Beyond a target drift ratio of 1%, increases in deformation caused widening of existing cracks rather than formation of new cracks. Spalling of the concrete at the base of the walls was clearly visible during the cycle to a target drift ratio of 2% for Specimens M60 and M115 and 1.5% for the other specimens. After that, relative displacement between the specimen and concrete base block became increasingly apparent as the number of loading cycles increased. Eventually, concrete along the base of the wall severely deteriorated (Fig. 7), which compromised the ability of the wall to transfer shear into the foundation. At final state, Specimens H60, H115, and H60X, the walls subjected to the higher shear stress demands, exhibited more extensive deterioration along the base of the wall than the walls with smaller shear demands despite undergoing fewer loading cycles.

Testing of Specimens M60 and M115 was terminated during the first two cycles to a target drift ratio of 4%. Significant loss of strength associated with damage at the base of the wall caused the test of Specimen M60 to be terminated after the second cycle, whereas the test of Specimen M115 was terminated in the first cycle after all six longitudinal bars on the east side of the specimen had fractured (Fig. 7(b)). Bar fracture was noted when Specimen M115 was subjected to the second and third cycles to a target drift ratio of –3%. Although the specimen still carried approximately 60% of its peak strength when loaded to a target drift ratio of 4% (the fractured longitudinal bars were on the compression side), effectively all strength was lost when the load was reversed (Fig. 6(b)).

Table 3—Summary of test results

Specimen	Loading direction	M60	M115	H60	H115	H60X
V_{peak}, kip (kN)	East	242 (1075)	248 (1104)	443 (1969)	406 (1808)	439 (1954)
	West	252 (1122)	234 (1043)	374 (1665)	387 (1723)	378 (1683)
$\frac{V_{peak}}{A_{cv}\sqrt{f'_c}}$, psi	East	5.16 (0.43)	5.40 (0.45)	8.88 (0.74)	8.16 (0.68)	9.00 (0.75)
	West	5.40 (0.45)	5.04 (0.42)	7.56 (0.63)	7.80 (0.65)	7.80 (0.65)
d_{peak}, %	East	0.65	0.93	0.66	1.40	0.89
	West	0.67	1.41	0.80	1.30	0.80
d_u, %	East	2.94	3.37	1.59	1.87	1.57
	West	2.41	3.05	1.64	1.92	1.56

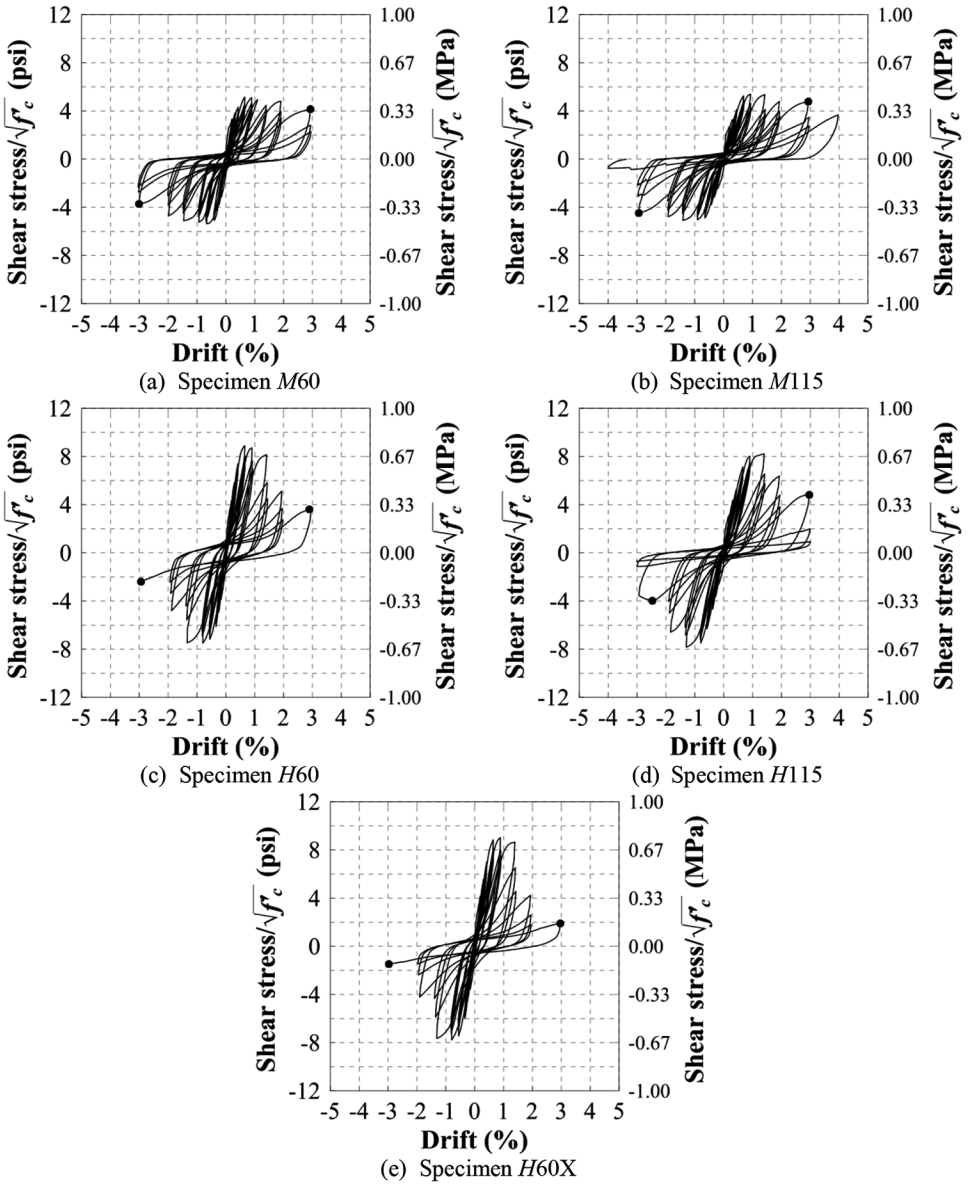

Fig. 6—Measured hysteresis.

The tests of Specimens H60, H115, and H60X were terminated before completion of three cycles to a target drift ratio of 3% due to significant loss of lateral resistance associated with serious damage at the interface between the specimen and concrete base block (Fig. 7).

Crack widths

Maximum crack widths were measured at the peak of the last cycle to each drift level in both loading directions. The maximum crack widths measured for each specimen (as an average of crack widths measured in each loading direction) are shown in Fig. 8. Horizontal crack widths were measured

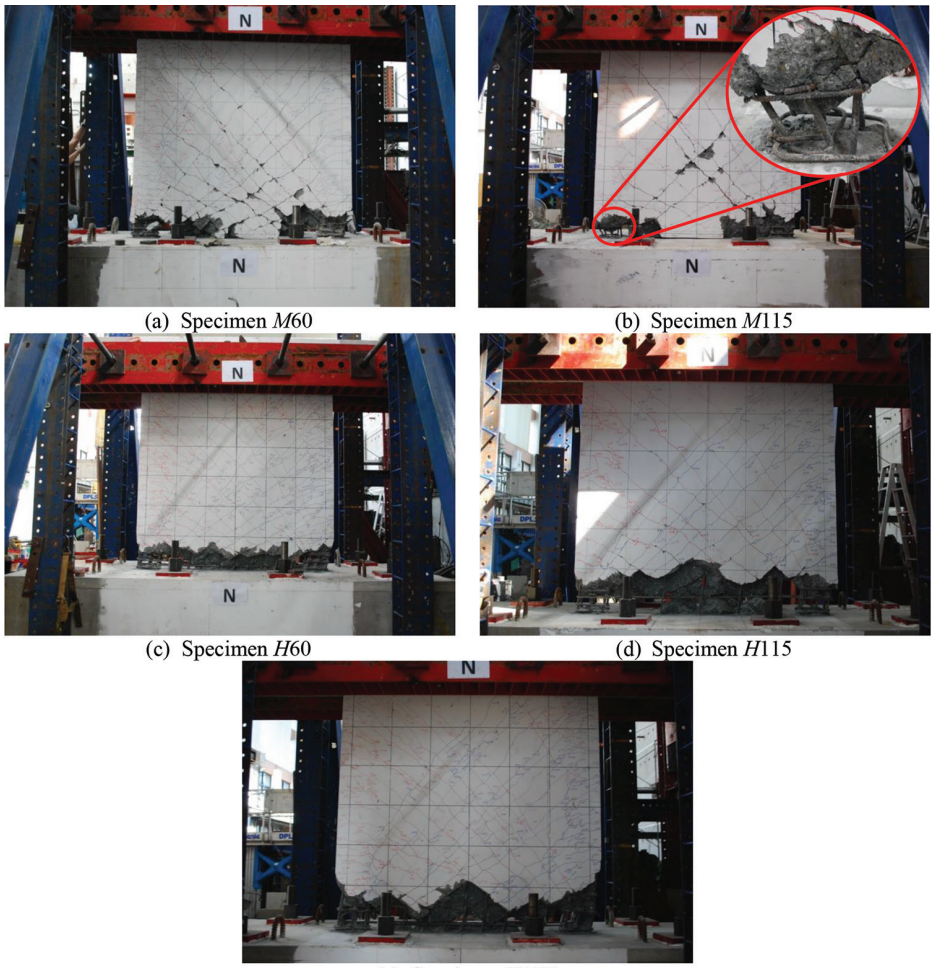

(a) Specimen *M*60 (b) Specimen *M*115

(c) Specimen *H*60 (d) Specimen *H*115

(e) Specimen *H*60X

Fig. 7—Final state of test specimens.

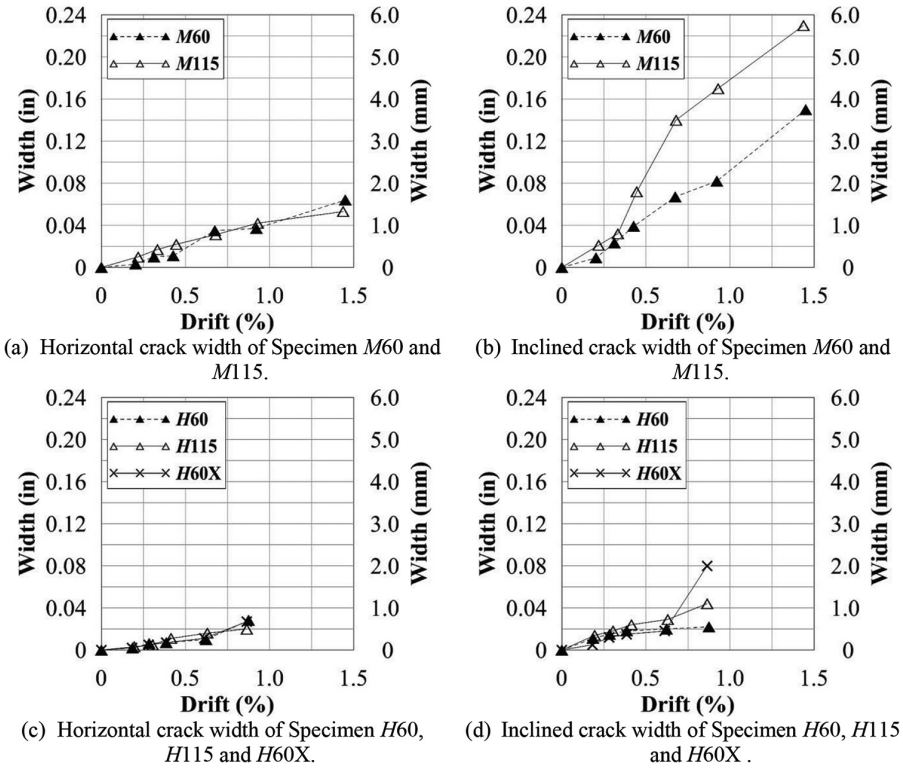

(a) Horizontal crack width of Specimen *M*60 and *M*115.

(b) Inclined crack width of Specimen *M*60 and *M*115.

(c) Horizontal crack width of Specimen *H*60, *H*115 and *H*60X.

(d) Inclined crack width of Specimen *H*60, *H*115 and *H*60X .

Fig. 8—Maximum crack widths of test specimens.

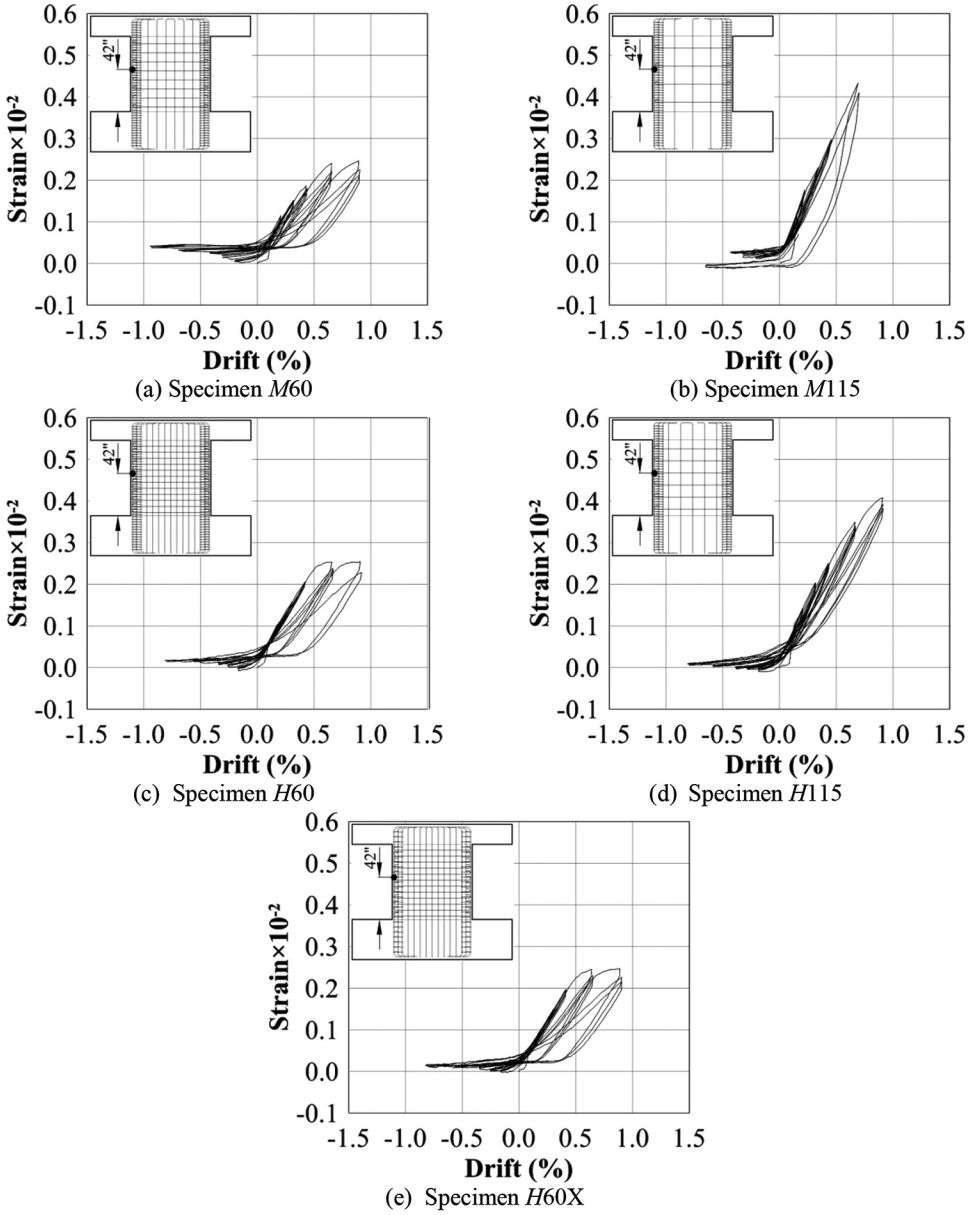

Fig. 9—Strains measured on exterior longitudinal bar.

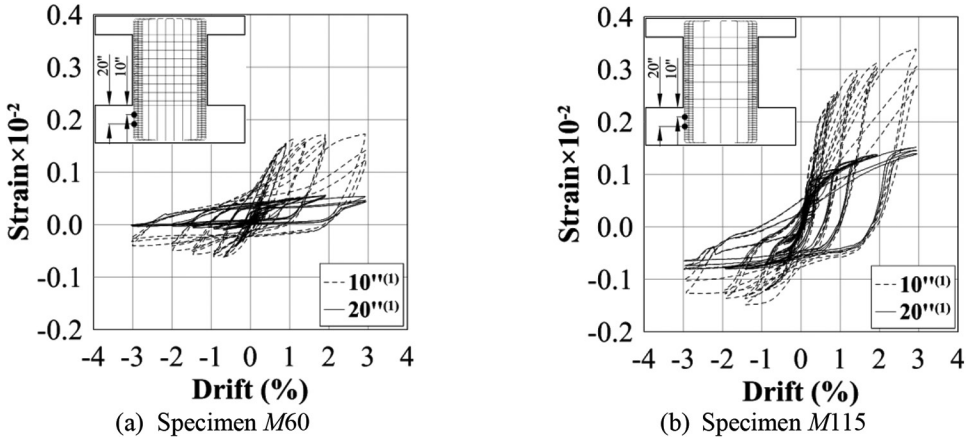

Fig. 10—Strain measured on exterior longitudinal bar within bottom concrete block.

on the east and west sides of the specimen and inclined crack widths were measured on the north side of the specimen.

The widths of inclined cracks were typically larger in Specimen M115, with $\rho_t = \rho_\ell = 0.0015$, than in Specimen M60, with $\rho_t = \rho_\ell = 0.0031$. Likewise, crack widths measured in Specimens H60 and H60X were similar, and smaller than in Specimen H115 for drift ratios less than 0.75%. It was observed that Specimens M60, H60, and H60X, reinforced with Grade 60 steel, had somewhat more numerous and closely spaced cracks than Specimens M115 and H115 (Fig. 7).

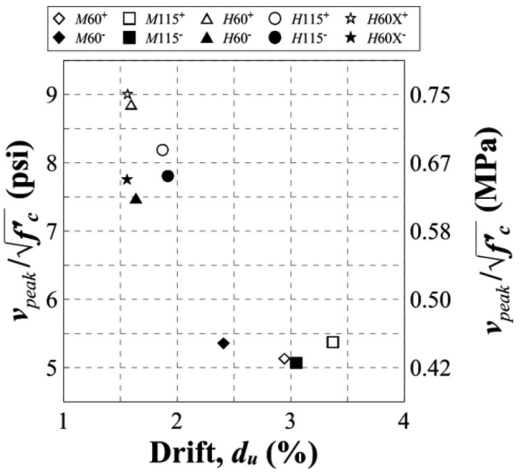

Fig. 11—Peak shear stress versus deformation capacity.

Reinforcement strains

Figure 9 shows plots of data from strain gauges on the longitudinal reinforcement in the special boundary element versus drift ratio (data are plotted for drift ratios up to 1% because strain gauge data were not consistently recorded for larger drift ratios, perhaps due to damage to the gauge wires). Recorded strains exceeded the yield strain (0.0022 and 0.0039, for Grade 60 and 115) at the base of the wall and up to approximately mid-height in all specimens before completion of the 1% drift cycle.

Within the concrete base block, two strain gauges were installed on the exterior longitudinal reinforcement at 10 and 20 in. (250 and 500 mm) below the top face of the concrete base block. As shown in Fig. 10, results from the two strain

Table 4—Shear strength evaluation

Specimen	M60	M115	H60	H115	H60X	Mean
V_{peak}*, kip (kN)	252 (1122)	248 (1104)	443 (1969)	406 (1808)	439 (1954)	—
V_{peak}/V_{Mn}	1.10	1.13	1.08	1.11	1.07	1.10
V_{peak}/V_{Mpr}	0.89	0.92	0.88	0.92	0.87	0.90
V_{peak}/V_{n1}	0.91	0.97	0.84	0.87	0.84	0.89
V_{peak}/V_{n2}	0.82	0.84	0.78	0.79	0.77	0.80
V_{peak}/V_{n3}	1.98	2.02	1.86	1.90	1.85	1.92
V_{peak}/V_{n4}	1.44	1.46	1.61	1.59	1.61	1.54

*Larger value of two loading directions.

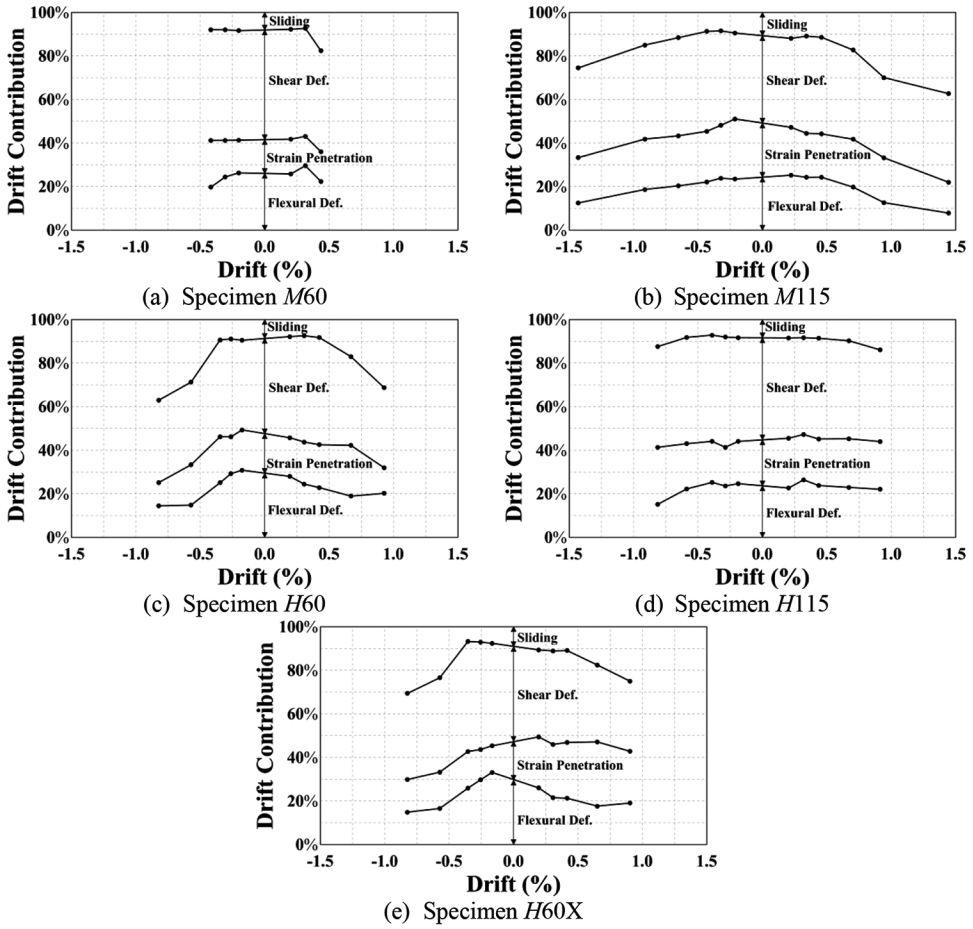

(a) Specimen *M*60; (b) Specimen *M*115; (c) Specimen *H*60; (d) Specimen *H*115; (e) Specimen *H*60X

Fig. 12—Deformation components.

gauges in Specimens M60 and M115 appear to consistently show a difference of approximately 1×10^{-3} and 1.5×10^{-3} for No. 7 Grade 60 steel and for No. 5 Grade 115 steel, respectively. Although not shown herein, similar results are observed in other specimens. This difference in strains over the 10 in. (250 mm) gauge length corresponds to an average bond stress of approximately 650 psi (4.5 MPa), or $8.5\sqrt{f_c'}$ psi ($0.7\sqrt{f_c'}$ MPa). Strains measured within the base block did not exceed the yield strain prior to completion of the cycles to a target drift ratio of 3%.

Some web reinforcement gauges, typically located near the center of the wall where inclined cracking was most significant, recorded strains exceeding yield strain in all five specimens. However, because only one specimen (M60) had recorded strains indicative of web reinforcement yielding near the boundary element, it was not possible to evaluate anchorage of horizontal web reinforcement.

DISCUSSION OF RESULTS

Deformation

The peak shear stress measured during the tests, divided by $\sqrt{f_c'}$, is plotted versus d_u in Fig. 11 for both loading directions (subscript "+" and "–" indicates positive and negative loading direction, respectively). The somewhat higher drift capacity (approximately 20% greater) associated with use of Grade 115 in place of Grade 60 is evident when Specimens M115 and H115 are compared to Specimens M60 and H60. The figure also shows the detrimental effect that high shear stress had on drift capacity. The results for Specimens H60 and H60X, which differed only in the maximum spacing of boundary element confinement reinforcement, are very close.

To investigate the influence of reinforcement grade on the relative importance of various deformation mechanisms, the contributions of strain penetration, sliding, flexure, and shear to specimen drift were calculated at the peak of the last cycle to each drift level (Fig. 12). The total drift ratio used to develop Fig. 12 corresponds to the relative displacement between the top row of markers and topmost markers on the base block (Fig. 4), corrected for rotation of the base block. Strain penetration and sliding, which respectively refer to rotation and lateral slip at the base of the wall, were calculated as the relative rotation and horizontal slip between the closely spaced markers adjacent to the wall-to-base block interface. Note that although some sliding does occur along cracks away from the base of the wall, the sliding component of drift reported in Fig. 12 only account for sliding at the base of the wall. Flexural deformations were calculated from the relative rotation between rows of markers. The remainder of the drift was attributed to shear deformations. Results are shown up to the drifts at which damage to the specimens compromised the deformation measurements.

As shown in Fig. 12, shear deformations and sliding accounted for more than half of the total drift of the specimens throughout the early cycles of each test. Comparing specimens using Grade 115 steel to specimens using Grade 60 steel, two differences in behavior can be observed. Strain penetration contributed approximately 50% more to the total drift in Specimens M115 and H115 than in Specimens H60 and H60X (no data for Specimen M60). This is likely due to the higher anchorage demands (per bar) associated with use of Grade 115 steel. A second observation is that an increase in base sliding occurred at drifts that coincided with yielding of the longitudinal reinforcement. Although sliding contributed approximately 8 to 10% of the total drift at drift ratios less than 0.3% in all specimens, an increase in the contribution of sliding (to more than 15% of total drift) was observed in Specimens M60, H60, and H60X at an imposed drift ratio of approximately 0.5%. Sliding in Specimens M115 and H115 did not contribute more than approximately 15% of total drift until a drift ratio of approximately 0.75%. These increases in sliding approximately coincided with the drifts at which recorded longitudinal reinforcing bars strains exceeded the yielding strain.

Strength

In Table 4, V_{peak} is given along with the ratio of V_{peak} to V_{Mn} and V_{Mpr}. Values given in Table 4 are calculated using measured material properties. The V_{peak}/V_{Mn} ratios indicate that the lateral strength of the specimens was governed by flexural yielding (which is consistent with Fig. 6 and strain gauge data). In addition, the data in Table 4 suggest that M_{pr} represents a safe estimate of the maximum forces that develop in squat walls limited in strength by longitudinal bar yielding.

Ratios of V_{peak} to the shear strengths calculated with Eq. (1) through (4) are also given in Table 4. Values of V_{peak}/V_{n1} and V_{peak}/V_{n2} show that the specimens were loaded close to, but always less than, the shear capacity calculated according to the ACI 318-14. That each specimen could be loaded so close to the calculated capacity without failing in either diagonal (web) or sliding shear before developing its flexure strength is an indication that use of Eq. (1) and (2) is safe for walls constructed with Grade 115 web reinforcement. In addition, deterioration of web shear strength after multiple cycles of load was delayed in specimens constructed with Grade 115. The V_{peak}/V_{n3} and V_{peak}/V_{n4} values were all greater than 1, with Eq. (3) (V_{n3}) resulting in the most conservative predictions (mean of $V_{peak}/V_{n3} = 1.9$). This was expected because Eq. (3) was proposed by Wood (1990) as a lower-bound estimate of squat wall strength. Equation (4), which was proposed by Gulec and Whittaker (2011) for estimating the mean shear strength of squat walls, also resulted in a conservative estimate, with a mean V_{peak}/V_{n4} of 1.5.

The shear capacity of Specimen H60X was not affected by the 50% reduction in the amount of confinement reinforcement in the boundary element (compared with the other specimens). It is important to emphasize that the transverse reinforcement spacing in Specimen H60X did not exceed $6d_b$ to delay buckling of longitudinal reinforcement.

Minimum web reinforcement ratio

Specimen M115, which was reinforced with Grade 115 steel, had $\rho_t = \rho_\ell = 0.0015$. This was less than the ACI 318-14 minimum of 0.0025 but provided approximately the same

$\rho_t f_y$ as in Specimen M60. Specimen M115 was loaded to 97% of its calculated web shear strength (based on ACI 318-14) without exhibiting a web shear failure, indicating that use of the low web reinforcement ratio (with adequate $\rho_t f_y$) did not compromise strength. However, Specimen M115 also exhibited the widest inclined cracking of any of the five specimens (Fig. 7). This was most likely due to the combined effects of the wide spacing of web reinforcement (18 in. [460 mm]), the high V_{peak}/V_{n1} value (near 1.0), and the low ρ_t.

SUMMARY AND CONCLUSIONS

Five large-scale squat wall specimens reinforced with either Grade 60 or 115 (413 or 785 MPa) steel bars were tested under reversed cyclic displacements. Design of the specimens was aimed at preventing shear failures prior to development of the probable flexural strength at the base of the wall. Based on the test results, the following conclusions are drawn:

1. Specimens reinforced with Grade 115 steel exhibited approximately 20% greater drift capacity than those reinforced with Grade 60 steel. The larger web reinforcement strains associated with use of HSS bars were not detrimental to lateral strength or drift capacity. Drift capacity, defined as a 20% loss in strength (from peak strength), was limited by severe damage to the concrete at the base of the wall.

2. Regardless of reinforcement grade, specimen strength was limited by flexural yielding. Although lateral loads never exceeded the shear strength calculated with ACI 318-14 equations, no evidence of their inadequacy was observed. Conservative estimates of strength were obtained using the equations proposed by Wood (1990) and Gulec and Whittaker (2011).

3. The use of web reinforcement ratios of 0.0015 for Specimen M115 (Grade 115 steel) did not compromise strength or drift capacity. At a drift ratio of 1%, the inclined cracks in Specimen M115 were approximately two times wider than the inclined cracks in Specimen M60 (Grade 60 steel) with a web reinforcement ratio of 0.0031.

4. The hysteresis results recorded for Specimens H60 and H60X (Grade 60 steel) were nearly identical despite Specimen H60X having 50% less boundary element confining reinforcement than Specimen H60. Spacing of boundary element confining reinforcement did not exceed $6d_b$ in either specimen.

5. Wall drift capacity decreased as shear-stress demands increased. An increase in shear stress from 5 to $9\sqrt{f_c'}$ psi (0.42 to $0.75\sqrt{f_c'}$ MPa) was associated with approximately 40% reduction in drift capacity.

AUTHOR BIOS

ACI member **Min-Yuan Cheng** *is an Associate Professor in the Department of Civil and Construction Engineering at National Taiwan University of Science and Technology, Taipei, Taiwan. He is a member of ACI Subcommittee 318-J, Joints and Connections (Structural Concrete Building Code), and Joint ACI-ASCE Committee 352, Joints and Connections in Monolithic Concrete Structures. His research interests include the behavior and design of reinforced concrete members subjected to earthquake-type loading.*

Shih-Ching Hung *received her BS and MS from the Department of Civil and Construction Engineering at National Taiwan University of Science and Technology in 2014 and 2016, respectively.*

ACI member **Rémy D. Lequesne** *is an Assistant Professor of civil, environmental and architectural engineering at the University of Kansas, Lawrence, KS. He is Secretary of Joint ACI-ASCE Committee 408, Bond and Development of Steel Reinforcement, and a member of ACI Subcommittee 318-J, Joints and Connections (Structural Concrete Building Code), and Joint ACI-ASCE Committee 352, Joints and Connections in Monolithic Concrete Structures. His research interests include the behavior of reinforced concrete and fiber-reinforced concrete members.*

Andrés Lepage, *FACI, is an Associate Professor in the Department of Civil, Environmental, and Architectural Engineering at the University of Kansas. He is a member of ACI Committees 335, Composite and Hybrid Structures; 374, Performance-Based Seismic Design of Concrete Buildings; 375, Performance-Based Design of Concrete Buildings for Wind Loads; and ACI Subcommittee 318-R, High-Strength Steel Reinforcement in Reinforced Concrete Design (Structural Concrete Building Code). His research interests include performance, analysis, and design of structural systems subjected to extreme loading events.*

NOTATION

A_{cv}	=	gross area of concrete bounded by ℓ_w and b_w
A_{vf}	=	total area of vertical reinforcement crossing horizontal shear plane
b_w	=	thickness of wall web
d_b	=	nominal diameter of smallest longitudinal reinforcing bar
d_{peak}	=	specimen drift ratio at peak load
d_u	=	specimen drift ratio at which lateral force dropped 20% below peak, derived from the force-displacement envelope
F_{vbe}	=	force attributed to vertical boundary element reinforcement (boundary element reinforcement area times f_y)
F_{vw}	=	force attributed to vertical web reinforcement (web reinforcement area times f_y)
f_c'	=	concrete compressive strength
f_t	=	steel tensile strength, measured in direct tension tests
f_y	=	yield stress of reinforcement
h_w	=	height of wall, measured from center of actuator force to top face of concrete base block
ℓ_w	=	length of wall
M_n	=	nominal flexural strength at base of wall
M_{pr}	=	probable flexural strength at base of wall determined using $1.25f_y$
P	=	axial force
V_{Mn}	=	M_n/h_w, shear force associated with M_n
V_{Mpr}	=	M_{pr}/h_w, shear force associated with M_{pr}
V_{n1}	=	nominal web shear strength, per Chapter 18 of ACI 318-14
V_{n2}	=	minimum nominal shear-friction strength, per Chapter 22 of ACI 318-14
V_{n3}	=	minimum shear strength, per Wood (1990)
V_{n4}	=	nominal shear strength, per Gulec and Whittaker (2011)
V_{peak}	=	maximum shear force measured during test
V_{test}	=	shear force measured during test
v_{peak}	=	V_{peak}/A_{cv}, maximum calculated shear stress
v_{test}	=	V_{test}/A_{cv}, calculated shear stress
α_c	=	aspect-ratio coefficient as defined by ACI 318-14, equal to 3.0 for $h_w/\ell_w \le 1.5$ and 2.0 for $h_w/\ell_w \ge 2$
ε_s	=	steel strain
ε_{sf}	=	elongation at fracture, steel strain corresponding to 10% drop from f_t (ASTM A370-14)
ε_{su}	=	uniform elongation, steel strain corresponding to peak stress
ρ_ℓ	=	vertical web reinforcement ratio (excludes boundary element)
ρ_t	=	horizontal web reinforcement ratio (excludes boundary element)

REFERENCES

ACI Committee 318, 2014, "Building Code Requirements for Structural Concrete (ACI 318-14) and Commentary (ACI 318R-14)," American Concrete Institute, Farmington Hills, MI, 519 pp.

Aoyama, H., 2001, *Design of Modern Highrise Reinforced Concrete Structures*, Imperial College Press, London, UK, 442 pp.

ASTM A370-14, 2014, "Standard Test Methods and Definitions for Mechanical Testing of Steel Products," ASTM International, West Conshohocken, PA, 50 pp.

Barda, F.; Hanson, J. M.; and Corley, W. G., 1977, "Shear Strength of Low-Rise Walls with Boundary Elements," *Reinforced Concrete in Seismic Zones*, SP-53, N. M. Hawkins and D. Mitchell, eds., American Concrete Institute, Farmington Hills, MI, pp. 149-202.

Gulec, C. K., and Whittaker, A. S., 2011, "Empirical Equations for Peak Shear Strength of Low Aspect Ratio Reinforced Concrete Walls," *ACI Structural Journal*, V. 108, No. 1, Jan.-Feb., pp. 80-89.

Gulec, C. K.; Whittaker, A. S.; and Stojadinovic, B., 2008, "Shear Strength of Squat Rectangular Reinforced Concrete Walls," *ACI Structural Journal*, V. 105, No. 4, July-Aug., pp. 488-497.

Moehle, J. P.; Ghodsi, T.; Hooper, J. D.; Fields, D. C.; and Gedhada, R., 2011, "Seismic Design of Cast-in-Place Concrete Special Structural Walls and Coupling Beams: A Guide for Practicing Engineers," *NEHRP Seismic Design Technical Brief No. 6*, National Institute of Standards and Technology, U.S. Department of Commerce, NIST GCR 11-917-11, 37 pp.

NIST GCR 14-917-30, 2014, "Use of High-Strength Reinforcement in Earthquake-Resistant Concrete Structures," NEHRP Consultants Joint Venture, Gaithersburg, MD, 231 pp.

Park, H.-G.; Baek, J. W.; Lee, J.-H.; and Shin, H.-M., 2015, "Cyclic Loading Tests for Shear Strength of Low-Rise Reinforced Concrete Walls with Grade 550 MPa Bars," *ACI Structural Journal*, V. 112, No. 3, May-June, pp. 299-310. doi: 10.14359/51687406

Paulay, T.; Priestley, M. J. N.; and Synge, A. J., 1982, "Ductility in Earthquake Resisting Squat Shearwalls," *ACI Journal Proceedings*, V. 79, No. 4, July-Aug., pp. 257-269.

Wood, S. L., 1990, "Shear Strength of Low-Rise Reinforced Concrete Walls," *ACI Structural Journal*, V. 87, No. 1, Jan.-Feb., pp. 99-107.